SSC22-VII-03

Attitude Determination with Self-Inspection Cameras Repurposed as Earth Horizon Sensors

Atilla Saadat
Space Flight Laboratory, University of Toronto Institute for Aerospace Studies
4925 Dufferin Street, Toronto, Ontario, Canada, M3H 5T6; +1 (226) 506-3830
asaadat@utias-sfl.net

Faculty Advisor: Robert E. Zee
Space Flight Laboratory, University of Toronto Institute for Aerospace Studies

ABSTRACT

Attitude determination for small satellites is a vital aspect of spacecraft operations. Earth Horizon Sensor(s) (EHS) are one of many sensors used in on-orbit attitude estimation. A conventional EHS captures infrared images of the Earth's horizon and estimates the nadir vector in the spacecraft body frame, using the Earth's curvature and prior knowledge of the spacecraft's orbit. However, the design and test of new sensors increase mission cost and development time, while some spacecraft may not be able to accommodate such dedicated sensors. Therefore, it is beneficial if existing onboard optical sensors could be repurposed as effective EHS. The Space Flight Laboratory has previously designed and launched the NorSat-2 spacecraft, equipped with the Miniature Vehicle Inspection Camera (mVIC) for antenna deployment inspection. This paper proposes a generalized nadir vector estimation methodology using simulation images from an optical sensor such as the mVIC, which was not originally designed as an EHS. Nadir vector estimation accuracy with software-generated sensor images is discussed and demonstrates the viability of the mVIC to be used as an EHS.

INTRODUCTION

For spacecraft to accurately conduct on-orbit mission operations, the Attitude Determination and Control Systems (ADCS) must meet the pointing requirements of onboard payloads and communication antennas. Spacecraft in Low Earth Orbit (LEO) use a combination of attitude determination sensors to meet mission requirements, which may include fine sun sensors, magnetometers, rate sensors, star trackers and Earth Horizon Sensor(s) (EHS)[1,2]. A conventional EHS captures infrared images of the Earth's horizon and estimates the nadir vector in the spacecraft body frame, using the Earth's curvature and prior knowledge of the spacecraft's orbit. Within this context, the nadir vector is the unit vector in the direction opposite to the orbit position vector. This EHS vector measurement can help improve overall three-axis attitude estimates from existing vector sensors, such as fine sun sensors or magnetometers, or provide a full three-axis solution if only one other vector measurement is available. However, the design and testing of new sensors increase mission costs and development time. Some spacecraft may also not be able to accommodate dedicated EHSs due to structural constraints. For this reason, it would be valuable if existing onboard optical sensors could be repurposed as an effective EHS. If the accuracy and performance of these sensors are deemed viable and meet system requirements related to attitude determination, this would benefit both on-orbit and in-development spacecraft missions without a dedicated Earth horizon sensor.

Many researchers have investigated the implementation and development of EHS for spacecraft nadir vector estimation. Most commonly, infrared camera sensors are utilized in EHS, as the infrared spectrum allows for nadir estimation during the eclipse stages of a spacecraft's orbit. For example, Nguyen et al. investigate an EHS design with an analytical nadir estimation approach[4]. The spacecraft used two infrared EHS with a 4° periodic low-frequency attitude disturbance to collect images for nadir determination, achieving an error of 0.16° and root-mean-square-error (RMSE) of 0.18°. Van Rensburg demonstrates an infrared imager is chosen and a "sub-pixel" edge detection algorithm using line fitting[5], with a horizon sensor estimation accuracy of <0.0811° (1σ) in pitch and <0.2944° (1σ) in roll axes. Dol Bahar et al. designed a CMOS horizon sensor using a circle-fitting centroid estimation algorithm[6], however, the calibrated accuracy (not explicitly stated) did not meet the intended accuracy of below 0.1° over the full Field of View (FOV). Commercial off-the-shelf (COTS) EHS are also

prevalent and available for purchase, ready for integration onto new spacecraft missions. CubeSpace, a commercial satellite hardware company, produces two types of EHS: CubeSense[7], a CMOS-based EHS and FSS with <0.2° (3σ) accuracy with a 180° FOV, and CubeIR[8], an infrared-based EHS with <1.5° (3σ) accuracy. Based on the past literature and COTS EHS, an error range of 0.1-0.25° at the 95th percentile for nadir vector estimation accuracy can be approximated. This allows for a direct performance comparison with developed and in-development EHS, encompassing both infrared and CMOS sensor accuracy ranges.

The University of Toronto's Institute for Aerospace Studies (UTIAS) Space Flight Laboratory (SFL) has previously designed and launched the NorSat-2 spacecraft, a maritime-monitoring microsatellite built for the Norwegian Space Agency (NOSA)[3]. It is equipped with the Miniature Vehicle Inspection Camera (mVIC), shown in Figure 1, which uses three CMOS sensors for Yagi antenna deployment inspection. Since the mVIC's sole purpose is antenna deployment verification, it has no additional operational usage after deployment. The goal of this preliminary study is to investigate the use of the mVIC beyond its original design purpose as an effective EHS, both for future SFL missions and current on-orbit SFL spacecraft equipped with the mVIC. There are three manners by which the mVIC data could be used to further increase attitude determination performance:

G1. Improve on-orbit attitude determination in sunlight by adding a supplementary vector measurement
G2. Improve whole orbit attitude determination on the ground through downlinked and post-processed mVIC data
G3. Enable full three-axis on-orbit attitude determination in eclipse by adding a supplementary vector measurement

An initial set of EHS accuracy requirements was determined based on past SFL missions and attitude sensor performances, shown in Table 1.

Table 1: Initial EHS design requirements for the mVIC

Requirement	Description
EHS-R001	The mVIC-derived vector measurements **shall** have an accuracy <10° (95th percentile)
EHS-R002	The mVIC-derived vector measurements **should** have an accuracy <5° (95th percentile)

Although the literature and COTS accuracy previously stated has a higher accuracy range, the requirements in Table 1 dictate the efficacy of the EHS outlined for this study, as the mVIC is primarily used on SFL satellite missions with related attitude determination requirements.

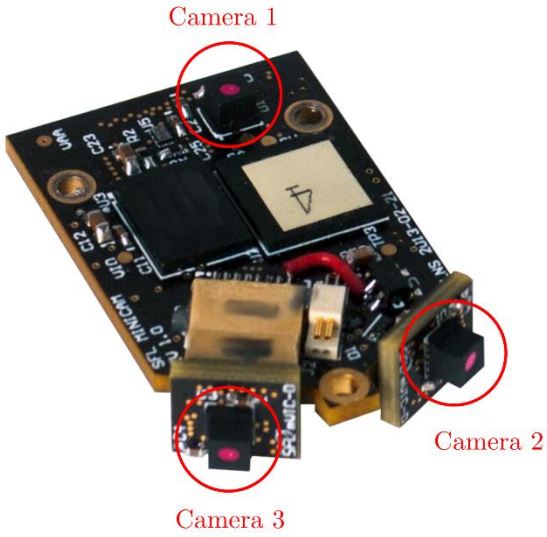

Figure 1: mVIC with three CMOS Sensors[9]

METHODOLOGY

The development of a methodology to test a CMOS-based EHS is first explored in detail through simulation. The simulation environment allows for rapid generation of orbital/attitude data and facilitates data generation for algorithm validation in a wide variety of operational scenarios. The software has also been developed in a generalized and modular manner, such that any spacecraft mission may validate EHS performance. In this section, we define the methodology to test and validate an EHS in software, with NorSat-2's mVIC as a case study in the subsequent section.

Simulation Environment and Image Generation

Analytical Graphics Inc. (AGI) Systems Tool Kit (STK) was chosen as the simulation environment for EHS development, as it provides multiple features for software-based algorithm tests and validation. STK allows for satellite object generation with set orbital parameters and attitude profiles (either as static orientations relative to a reference frame or attitude files created from spacecraft telemetry data). Tied to this data, a spacecraft 3D model can be imported for better visualization of spacecraft geometry with reference axes, sensor boresight vectors, horizon vector tracing, and the estimated nadir vector. In STK, the Electro-Optical and Infrared (EOIR) sensor object was selected to simulate the camera sensor and generate images in the spacecraft's instantaneous simulation environment. The sensor's location and orientation relative to the spacecraft's body frame were also programmatically set.

The EOIR sensor object is then assigned parameters to match the spacecraft's camera sensor spatial, spectral, optical, and radiometric properties. STK's Python API is also used to automate the data exchanges between STK and the nadir estimation software.

To ensure the generated simulation images contain the Earth's horizon for analysis, the Obscuration tool in STK is integrated with the automation scripts. Using this feature, images from the sensor are only captured if the Earth is known to obstruct between 1% and 99% of the total image area, thus only producing images with the Earth's horizon in view.

Image Preprocessing and Edge Detection

From the STK environment, multiple EHS simulation images are produced with a known timestamp. For a given image, several preprocessing steps are performed to produce an array of horizon vectors in the body frame, which will then be used as the input for nadir vector estimation.

First, the RGB image is converted into a greyscale image. Next, the image is converted into a binary image with a constant pixel value threshold, τ_p, set to define the binary cutoffs for the image where the white pixels represent the Earth and the black pixels represent deep space.

The final preprocessing step is edge detection. Although various edge detection algorithms exist, the Canny edge detector was chosen due to its performance, computational load, and ease of implementation into the software stack[5]. Open Source Computer Vision Library (OpenCV) was utilized to perform the Canny edge detection in the Python environment, set hysteresis thresholds, and produce an array of pixel coordinates corresponding to the detected horizon edge.

Given the set of N horizon pixel coordinates generated through preprocessing, various coordinate frame transformations are required to correlate pixels to horizon vectors defined in the body frame of the spacecraft[5]. These transformations are defined in Equations (1)-(4),

$$H_i = \begin{bmatrix} h_{y_0} & h_{x_0} \\ \vdots & \vdots \\ h_{y_N} & h_{x_N} \end{bmatrix} \tag{1}$$

$$H_c = H_i - \begin{bmatrix} \frac{h}{2} & \frac{w}{2} \end{bmatrix}_{N\times 2} \tag{2}$$

$$H_s = \begin{bmatrix} H_c & \left[\frac{f}{p_s}\right]_{N\times 1} \end{bmatrix} \tag{3}$$

$$H_b = \mathcal{R}_{sb} H_s^T \tag{4}$$

where h is the height of the image, w is the width of the image, f is the image focal length, p_s is the pixel size, and $\mathcal{R}_{sb}$ is the rotation matrix from the sensor frame, $\mathcal{F}_s$, to the spacecraft's body frame, $\mathcal{F}_b$.

First, the horizon pixels are stacked into the image frame, $\mathcal{F}_i$, as the matrix H_i, as defined in Equation (1). This matrix is then offset to the center frame, $\mathcal{F}_c$, such that all the horizon pixel coordinates are relative to the center of the image, with the matrix H_c, as defined in Equation (2). The sensor frame, $\mathcal{F}_s$, sets the origin at the sensor and H_s is defined in this frame in Equation (3). This adds a third dimension to the horizon pixels by setting a z-axis distance with the sensor focal length and pixel size. Last, the rotation matrix $\mathcal{R}_{sb}$ is applied to map the horizon vectors H_s in the spacecraft's body reference frame, $\mathcal{F}_b$, as defined in Equation (4). The various reference frames with their relation to a captured image are illustrated in Figure 2. Similar to the horizon vectors, a "space" matrix, S_b, is also defined, consisting of m randomly chosen vectors that point to deep space. This matrix is used to calculate biasing term in the cost function, detailed in the next subsection. The space vectors follow the same transformations in Equations (1)-(4), replacing the horizon pixel locations and vectors, H_i, with the space vectors, S_i.

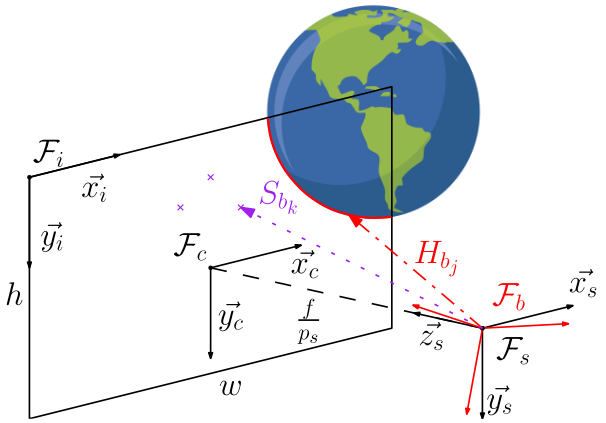

Figure 2: Image to Body Reference Frame Transformations

Nadir Vector Estimation Algorithm

Nadir vector estimation requires a known and constant Earth horizon angle, denoted by ρ. Figure 3 graphically represents the simplified angular relations of the Earth

and spacecraft, illustrating the Earth horizon angle[1]. The horizon angle as seen by an in-orbit spacecraft may also be larger than the angle to the horizon at the surface of the Earth, due to the atmospheric height at the horizon. Therefore, on-orbit images used for nadir estimation would be estimating ρ', shown in Equation (5),

$$\sin \rho' \cong \frac{R_e + d_a}{R_e + A_{sat}} \tag{5}$$

where R_e is the constant radius of the Earth, d_a is the height of the atmosphere, and A_{sat} is the altitude of the spacecraft.

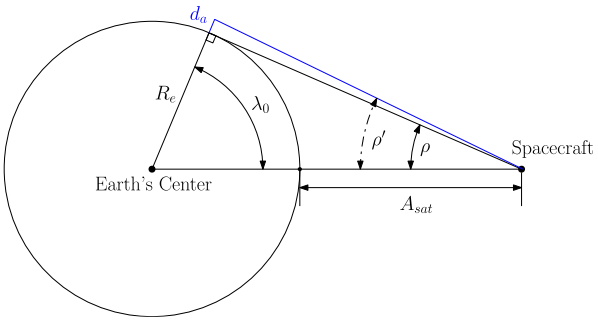

Figure 3: Definition of Angular relations between a Satellite, Earth, and the visible Horizon

With an Earth horizon angle defined, the nadir vector estimate can be calculated as the solution to the minimization problem using the constant horizon angle, shown in Equation (6). The cost function, defined in Equation (7), estimates an azimuth, ψ, and elevation angle, ϵ, that corresponds to the nadir vector estimate in the spacecraft's body frame, $\mathcal{F}_b$, as shown in Figure 4. The selection of these two independent angles parameterizes the nadir vector solution to allow for an unconstrained minimization problem. The term $J(\epsilon, \psi)$ represents the L^2 norm of the list of differences between two angles: constant Earth horizon angle and the angles produced by the nadir vector solution, $\vec{n}_b$, and detected horizon vectors in the spacecraft's body frame.

The augmented cost function in Equation (6) also has an additional nadir biasing term, ε, that was introduced to bias the solution towards the true nadir vector. The bias term is shown in Equation (9), where S_b is a $m \times 3$ matrix of uniformly random space vectors, η is a chosen angular offset for the Earth horizon angle, and $card$ is the cardinality function (i.e., the total number of items in a set). This term yields the number of space vectors, within a randomly chosen set, that has a larger angle to the nadir estimate than the known Earth horizon angle. The offset term η ensures vectors close to the Earth's horizon are not considered. The purpose of this term is to promote a solution closer to the true nadir vector and away from the vector pointing towards space with the same angular residual as the true nadir vector solution.

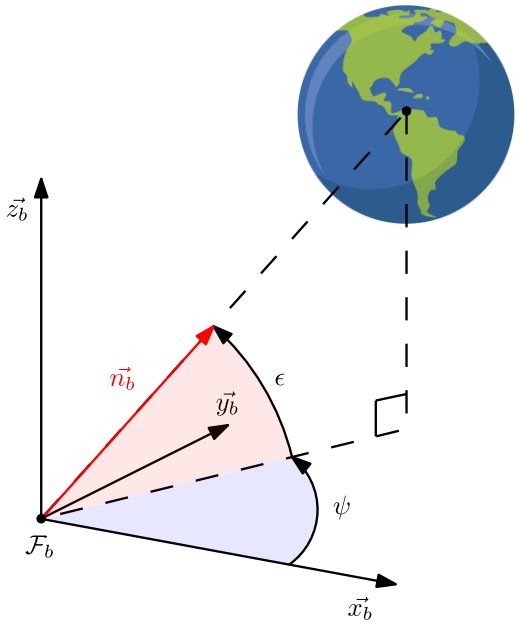

Figure 4: Nadir Vector Estimate Angle Definitions[5]

$$\arg\min_{\epsilon,\psi \in \mathbb{R}} \zeta_b(J(\epsilon,\psi),\varepsilon) \tag{6}$$

$$J(\epsilon,\psi) = \|(H_b \cdot \vec{n}_b) - cos(\rho')\|_2 \tag{7}$$

$$\zeta_b(J(\epsilon,\psi),\varepsilon) = \begin{cases} J(\epsilon,\psi), & \varepsilon = 0 \\ -\dfrac{\varepsilon}{J(\epsilon,\psi)}, & \varepsilon > 0 \end{cases} \tag{8}$$

$$\varepsilon = \text{card}\left(cos^{-1}(S_b \cdot \vec{n}_b) < (\rho' + \eta)\right) \tag{9}$$

Three candidate optimization methods were selected for solving the minimization problem: limited-memory Broyden–Fletcher–Goldfarb–Shanno (L-BFGS), least-squares, and a hybrid particle swarm optimization (PSO) method with sequential least-squares programming (SLSQP) and reflect bounding method. After various trials with the performance of the listed minimization methods, the PSO algorithm was chosen for its nadir estimate accuracy, repeatability, and efficacy due to its use of stochastic methods to avoid local minima alongside deterministic gradient-based optimization.

CASE STUDY

A case study was conducted with the above methodology using the NorSat-2 mission specifications in STK, such as the geometric model, orbital parameters, mVIC relative position/orientation, and sample attitude files. The mVIC, shown in Figure 1, has three CMOS sensors to view the deployment of the antennas. mVIC properties[9] are shown in Table 2, listing the various parameters used to define the STK EOIR sensor object for image generation. Saturation was enabled for the EOIR images to match effects illustrated in past on-orbit mVIC images from NorSat-2, seen in Figure 6 displaying a sample image with part of the antenna captured in the frame. Since the NorSat-2 image capture time offset was not known during deployment, this image (along with other captured deployment verification images) cannot be used for estimate validation with the coupled attitude data.

Table 2: mVIC Specifications with utilized STK EOIR parameters

Category	Specification	Value	STK
Physical	Mass	5 g	
	Dimensions	20 × 30 mm	
	Power Consumption	60 mW	
	Number of Cameras	3	
Optical	Focal Length	1.15 mm	✓
	Field of View	40°V × 52°H	✓
	f-number	3.0	✓
	Focus Type	Fixed	
	Depth of Field	30 cm to ∞	
System	Frame Rate	1 frame / 30 sec.	
Sensor	Array Size	640 × 480 px.	✓
	Array Type	Bayer BGGR	
	Bit Depth	8	
	Pixel Size	1.75 × 1.75 nm	✓
Spectral	Spectral Band Edge Wavelengths (Full Spectrum)	400 – 700 nm	✓

With the STK model shown in Figure 5, all simulation parameters are defined for image generation purposes. NorSat-2's actual orbit and attitude data collected from 18 Jul 2017 00:00:26.000 UTC to 19 Jul 2017 23:59:26.000 UTC was used in the simulation environment. This input matches the simulation scenario to a nominal attitude case seen on the NorSat-2 mission. Within the start and end of this timespan, multiple images were generated at 5-minute intervals for direct use in nadir vector estimation and validation. For each image, the epoch time and true nadir vector in the body frame were recorded for estimation error calculations. The bias term parameters m and η were set to 1000 and 1°, respectively, to provide a sufficient amount of space vectors for the bias term with a small angular offset. For the calculation of ρ', A_{sat} was set to NorSat-2's orbital altitude and d_a was set to 0 km since EOIR images don't simulate atmospheric height and related effects.

Although the mVIC has three sensors onboard, only Camera 3 (shown in Figure 1) was defined in simulation to test the nadir vector estimation performance using a single mVIC image, without requiring a combined estimate from multiple images. A significant parameter that required iterative tuning was the constant pixel value threshold, τ_p, which was set to 150 based on its performance with horizon vector estimates.

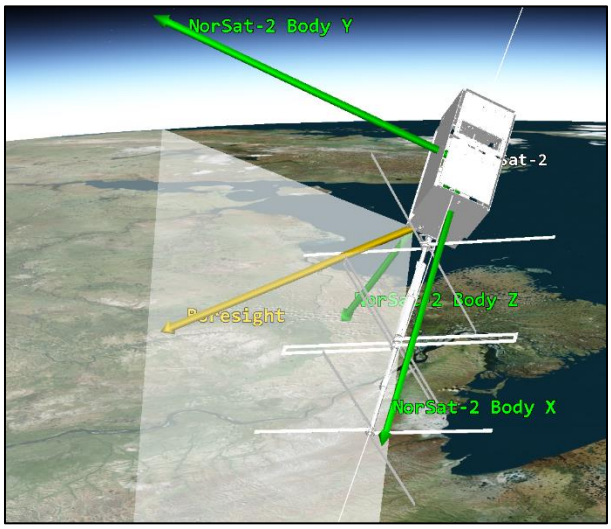

Figure 5: NorSat-2 simulation with the simplified CAD model, mVIC FOV, and Earth intersection

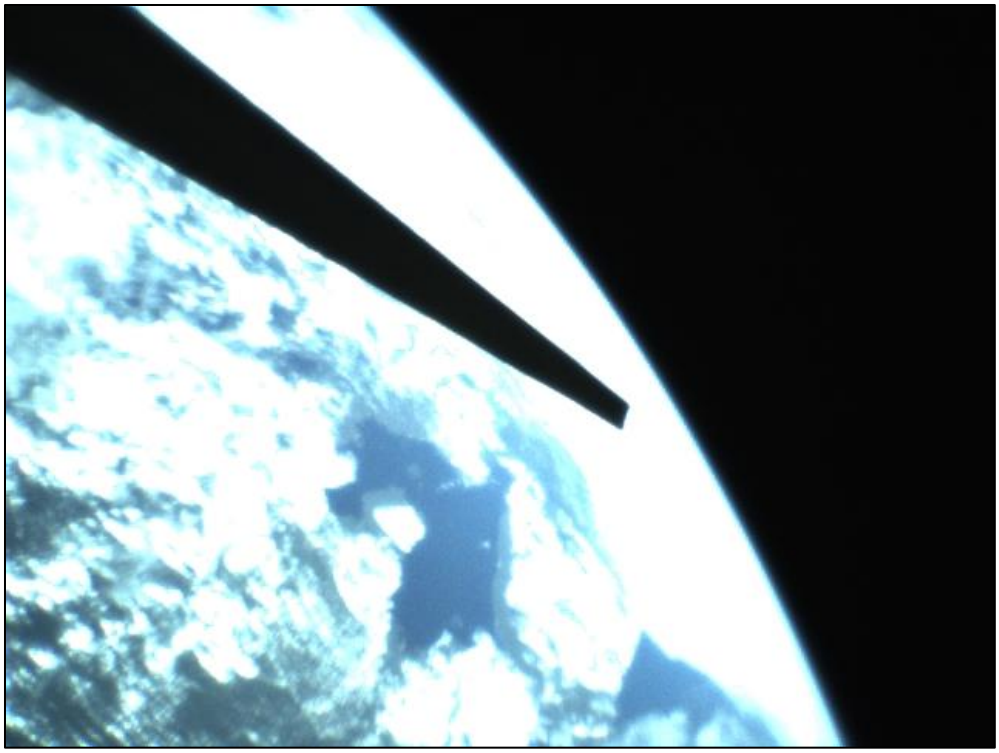

Figure 6: Sample mVIC image (Camera 3) taken from NorSat-2 on 19 Jul 2017

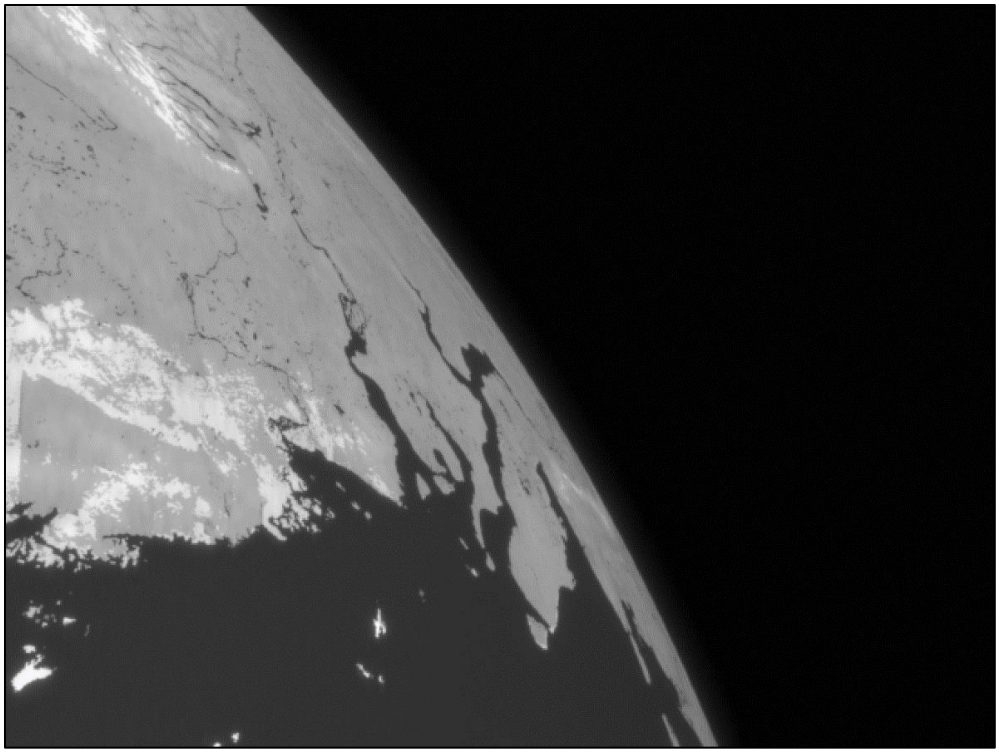

Figure 7: Sample mVIC EOIR image (Camera 3) – CaseTime 3602 - Full spectrum with no Saturation

Figure 8: Sample mVIC EOIR image (Camera 3) - CaseTime 3602 - Full spectrum with Saturation and Detected Horizon Edge

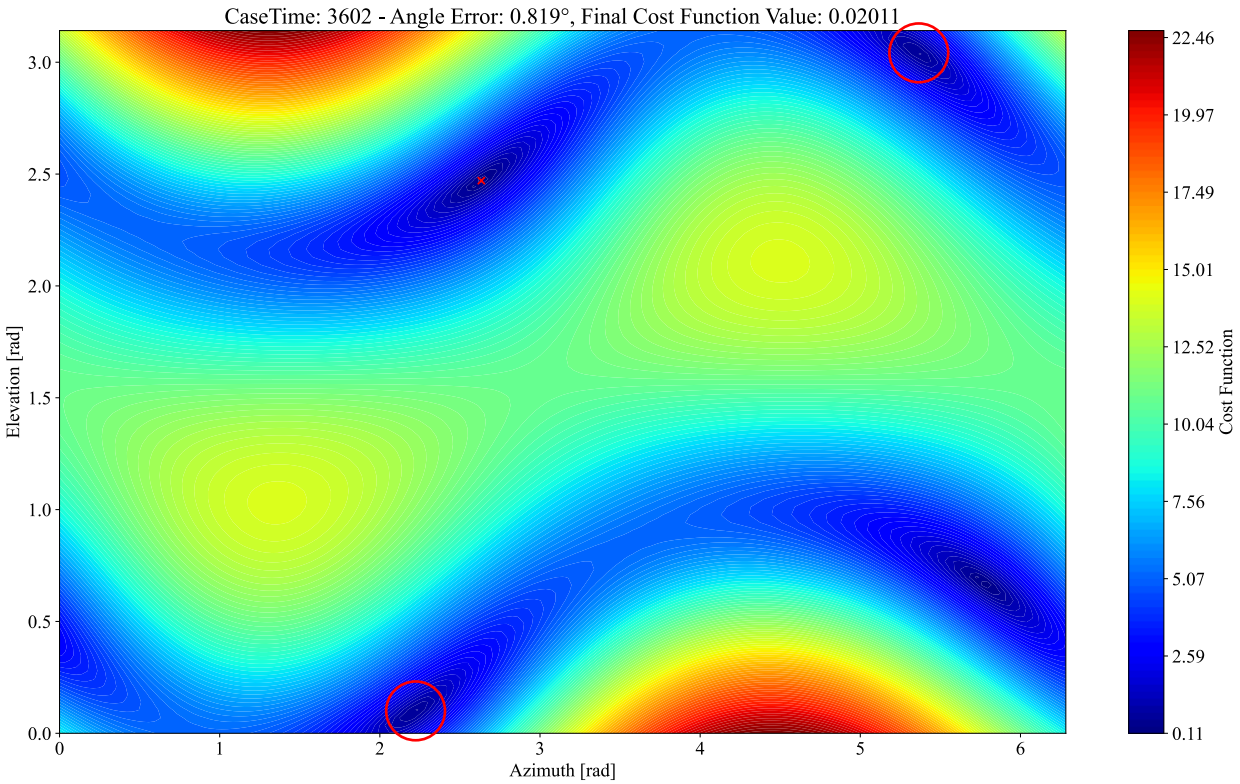

Figure 9: Cost Function Contour - CaseTime 3602 – Minimizing Equation (7) (without ε)

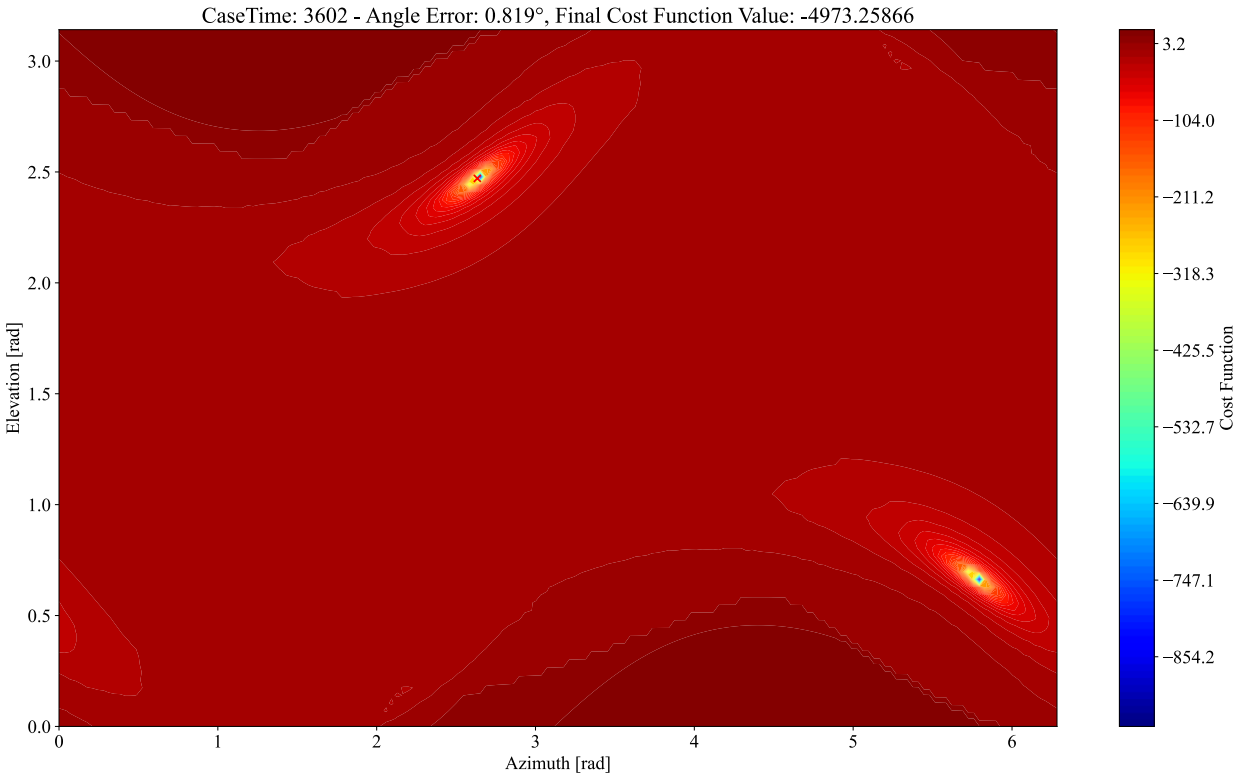

Figure 10: Cost Function Contour for CaseTime 3602 – Minimizing Equation (8) (with ε)

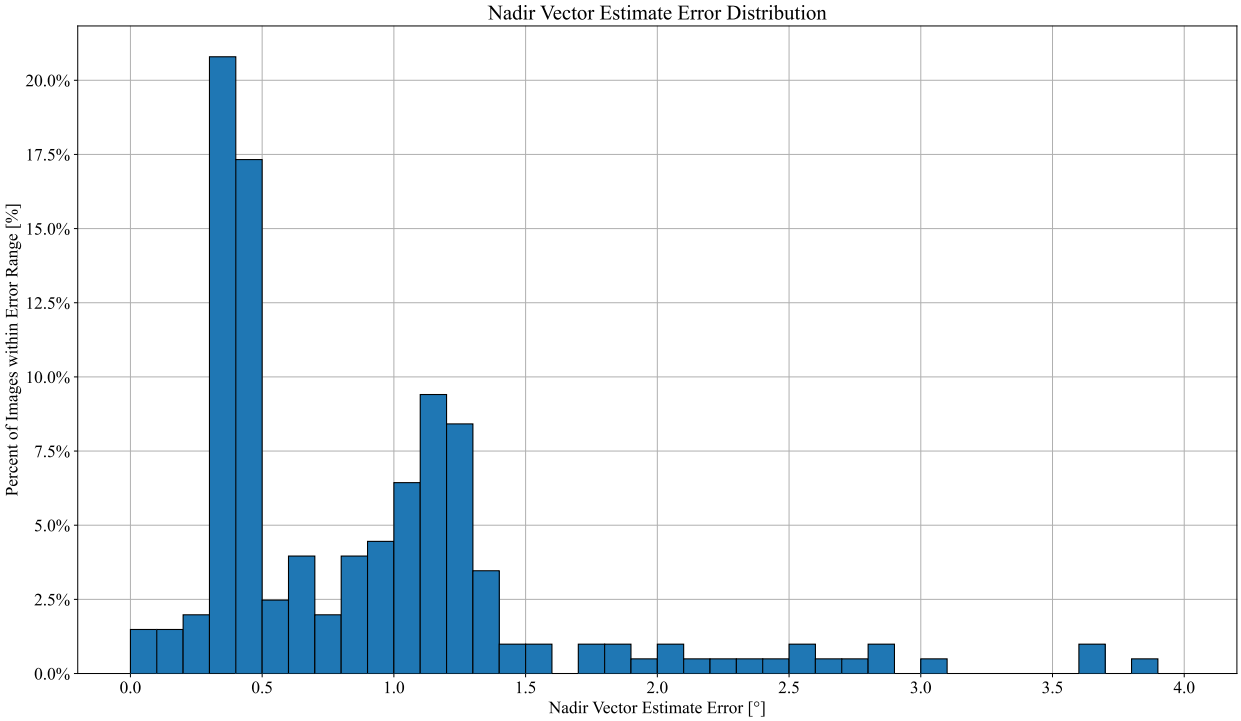

Figure 11: Nadir Vector Estimate Error Distribution of All Images Generated during the Timespan

RESULTS AND DISCUSSION

Running the case study yielded a set of over 200 mVIC simulation images to be utilized for analysis, each using the full-spectrum wavelength of the mVIC and with saturation enabled. Figure 7 illustrates a sample image at an instant in the timespan, CaseTime 3602, with saturation disabled. Figure 8 shows the same instance with saturation enabled, demonstrating similar visual effects of the Earth seen in Figure 6. Figure 9 shows the cost function contour when using Equation (7) as the minimization problem, while Figure 10 demonstrates the effect of the bias term, ε, when Equation (6) is used as the minimization problem. The difference in these graphs show the removal of the "mirrored" or false nadir vectors from the search space, highlighted with red circles. The addition of the bias term removes the local minima so that the PSO algorithm may reach the true global minima at the correct nadir solution. Without the need for prior attitude information, this method of attitude determination relies solely on the EHS image. The resulting nadir vector estimates from the images within the timespan produced the resulting error distributions graphed in Figure 11. The case study's numerical performance metrics are listed in Table 3.

Table 3: Case Study Results - Angular Error Metrics

Metric	Value
Mean	0.91°
RMSE	1.14°
Standard Deviation (σ)	0.69°
Accuracy at 95th percentile	2.42°

The listed accuracy performances do not currently contend with alternative infrared or COTS Earth horizon sensors (0.1-0.25° at 95th percentile). However, it does indicate that (in simulation) the mVIC meets the system requirements necessary for it to be utilized as an EHS for SFL's satellite missions. The accuracy requirements, listed in Table 1, are all satisfied and demonstrate promising attitude estimation performance if in-orbit images are analogous to simulation-based images. The results also satisfy design goal G2, as sufficient attitude determination is achieved through on-ground processing methods.

CONCLUSION AND FUTURE WORK

This paper discusses a methodology for testing and developing an EHS out of a repurposed spacecraft inspection camera. The methodology was introduced as a multistep process of generating simulation images of an on-orbit camera sensor, preprocessing the image for Earth horizon edge detection, and using minimization algorithms to estimate the spacecraft's nadir vector. A case study for this method was conducted demonstrating the results of the methodology using NorSat-2's mission and mVIC parameters. The performance of this method was shown to meet SFL requirements in simulation, suggesting the mVIC could be a viable EHS after the primary task of antenna deployment verification is completed.

Further work is planned to improve the simulation and on-orbit performance of the mVIC as an EHS. NorSat-2 TimeTag commands have been created to capture 50 images during a fine-pointing attitude maneuver. These images would provide a dataset for further tuning image preprocessing, edge detection, and method viability using in-situ images. With in-orbit mVIC images, antenna elements may block the horizon in certain attitudes, as seen in Figure 6. A large dataset of in-orbit images would provide the framework to develop algorithms to remove the antenna's influence in horizon edge detection, an effect that cannot be captured through simulation. The in-situ images also allow for simulation-based images to be validated as a viable substitute for testing, as they can be compared directly using the same orbit, attitude, and timestamp information. Additionally, with the performance of the estimation algorithm established, further improvements can be made to the robustness of the edge detection algorithm, both with simulation and on-orbit images.

The SFL EHS design goal G3 also requires multiple on-orbit images to provide a dataset to evaluate the practicality of EHS images in eclipse, another effect that is not fully captured in simulation, as gain tuning at specific spectrums could yield a detectable horizon with CMOS sensors. Design goal G1 also required the method to be further developed and optimized for use in flight code. Additionally, misalignment sensitivity analysis is to be done to assess its effect on nadir vector estimation accuracy.

ACKNOWLEDGEMENTS

The author would like to express deep and sincere gratitude to Dr. Robert E. Zee for providing the guidance and opportunity to conduct research and development on spacecraft at SFL, alongside many talented students and staff members. The author would also like to especially thank Niels Roth for productive discussions related to this research. Finally, the author would like to thank the collaboration of NOSA for the use of NorSat-2 images and eventual mission assets for further EHS development.

REFERENCES

1. J. R. Wertz, D. F. Everett, and J. J. Puschell, *Space Mission Engineering: The New SMAD*. Microcosm Press, 2011.

2. K. Sarda, C. Grant, M. Chaumont, S. Y. Choi, B. Johnston-Lemke, and R. E. Zee, "On-Orbit Performance of the Bright Target Explorer (BRITE) Nanosatellite Astronomy Constellation," in *28th Annual AIAA/USU Conference on Small Satellites*, Utah State University, Logan, Utah, 2014.

3. L. M. Bradbury, D. Diaconu, S. Molgat Laurin, A. M. Beattie, C. Ma, I. S. Spydevold, H. C. Haugli, R. E. Zee, J. Harr, and F. Udnæs, "NORSAT-2: Enabling advanced maritime communication with VDES," *Acta Astronautica*, vol. 156, pp. 44–50, 2019.

4. T. Nguyen, K. Cahoy, and A. Marinan, "Attitude determination for small satellites with Infrared Earth Horizon Sensors," *Journal of Spacecraft and Rockets*, vol. 55, no. 6, pp. 1466–1475, 2018.

5. H. M. van Rensburg, "An Infrared Earth Horizon Sensor for a LEO Satellite," M.S. Thesis, University of Stellenbosch, Matieland, South Africa, 2008.

6. M. Dol Bahar *et al.*, "Modular CMOS Horizon Sensor for Small Satellite Attitude Determination and Control Subsystem," in *20th Annual AIAA/USU Conference on Small Satellites*, Utah State University, Logan, Utah, 2014.

7. CubeSpace, "CubeSense," *CubeSpace*. [Online]. Available:https://www.cubespace.co.za/products/adcs-components/cubesense/.

8. CubeSpace, "Cubeir," *CubeSpace*. [Online]. Available:https://www.cubespace.co.za/products/adcs-components/cube-ir/.

9. C. B. Wheeler, "Adaptation of Commercial Off-the-shelf Camera Technology for Deployment Imaging and Inspection on Small Satellites,", M.S. Thesis, Aerospace Science and Engineering, University of Toronto, Toronto, Canada, 2017.